HHS Public Access

Author manuscript

Biochemistry. Author manuscript; available in PMC 2016 December 15.

Published in final edited form as:

Biochemistry. 2015 December 15; 54(49): 7222–7228. doi:10.1021/acs.biochem.5b01160.

Crystal Structure of Recoverin with Calcium Ions Bound to Both Functional EF-Hands

Ramasamy P. Kumar[1], **Matthew J. Ranaghan**[1], **Allen Y. Ganjei**[1], and **Daniel D. Oprian**[1,*]

[1]Department of Biochemistry, Brandeis University, Waltham, MA 02454

Abstract

Recoverin (Rv), a small Ca^{2+}-binding protein that inhibits rhodopsin kinase (RK), has four EF hands, two of which are functional (EF2 and EF3). Activation requires Ca^{2+} in both EF hands, but crystal structures have never been observed with Ca^{2+} ions in both sites; all previous structures have Ca^{2+} bound only to EF3. We suspected that this was due to an intermolecular crystal contact between T80 and a surface glutamate (E153) that precluded coordination of a Ca^{2+} ion in EF2. We constructed the E153A mutant, determined its X-ray crystal structure to 1.2 Å resolution, and show that 2 Ca^{2+} ions are bound, one in EF3 and one in EF2. Additionally, several other residues are shown to adopt conformations in the $2Ca^{2+}$-structure not seen previously and not seen in a second structure of the E153A mutant containing Na^{+} instead of Ca^{2+} in the EF2 site. The side-chain rearrangements in these residues form a 28 Å long allosteric cascade along the surface of the protein connecting the Ca^{2+}-binding site of EF2 with the active-site pocket responsible for binding RK.

Recoverin (Rv) is a small (23kDa) calcium (Ca^{2+}) binding protein of the neuronal calcium sensor (NCS) family [1, 2] found in rod photoreceptor cells of vertebrate retina. Under *in vitro* conditions, when Ca^{2+} concentration is high, Rv inhibits rhodopsin kinase (RK) to prolong activation of the visual pigment rhodopsin [3-5]. Rv binds to the N-terminal helix of RK [6, 7], an amphipathic helix also recognized by rhodopsin [8]. This interaction prolongs activation by inhibiting the ability of RK to phosphorylate rhodopsin.

The first crystal structure of Rv, determined over 20 years ago, revealed a compact arrangement of four EF hands, only one of which (EF3) had a bound Ca^{2+} ion [9]. EF3 exhibits the canonical pentagonal bipyramidal geometry for binding a Ca^{2+} ion. The seven atoms coordinating the Ca^{2+} ion come from an axial water molecule (oxygen with spatial position −X) and five residues in the EF hand loop. The coordinating atoms include one oxygen atom each from Asp110 (X), Asp112 (Y), Asn114 (Z), and Thr116 (main chain carbonyl oxygen; −Y), and two oxygen atoms from Glu121 (−Z). The observation of only one Ca^{2+} ion bound in the crystal structure is perplexing because Rv in solution is well

*To whom correspondence should be addressed: Daniel D. Oprian, Department of Biochemistry, Brandeis University, 415 South St, Waltham, MA 02454. Tel.: 781-736-2322, Fax: 781-736-8487, oprian@brandeis.edu.

[1]The authors declare no competing financial interest

[2]The atomic coordinates and structure factors (codes 4YI8 and 4YI9) have been deposited in the Protein Data Bank.

SUPPORTING INFORMATION

Ca^{2+} titration in the presence of 1.5 M NaCl

known to bind two Ca^{2+} ions, one in EF2 and one in EF3 [10, 11], and coordination of Ca^{2+} at both EF2 and EF3 sites is required for binding RK [12, 13].

In the intervening years since the first structure, Rv has never been crystallized with Ca^{2+} bound to both sites. All of the crystal structures exhibit a nearly identical protein conformation containing one Ca^{2+} ion bound to EF3 with the same heptacoordinate geometry [13-15]. Interestingly, the Ca^{2+}-free conformation of the EF2 loop is in an open conformation in all Rv structures except a mutant (Δ191-202) with a truncated C-terminal tail [15], where the loop is found to be in a partially closed conformation.

We searched existing Rv structures for crystal contacts that might cause interference with the EF2 loop and identified an intermolecular contact (i.e., hydrogen bond) between T80 (−Y) in the EF2 loop and E153 in the entering helix of the non-functional EF4 (Fig. 1). The hydrogen bond appears to prevent rotation of the D78 (Z) sidechain suggesting that the T80-E153 interaction may prevent Ca^{2+} coordination in EF2. To explore how this interaction might modify binding of Ca^{2+} to the protein in crystals, we created, characterized, and crystallized the E153A Rv mutant, leaving residues of EF2 unaltered.

We show here that the E153A mutation has minimal effect on the ability of Rv to bind Ca^{2+} and RK. However, the crystal structure of the E153A mutant, determined at 1.2 Å resolution, contains several differences with respect to the wild-type (WT) protein, most notably, two bound Ca^{2+} ions, one each in EF2 and EF3, both with canonical pentagonal bipyramidal geometry expected for heptacoordinated Ca^{2+} in EF hands. Several other amino acid residues stretching from EF2 to the N-terminus of the protein adopt conformations not observed in previous crystal structures of Rv.

We also determined the structure of E153A Rv containing a hexacoordinated Na^+ ion in EF2 and a heptacoordinated Ca^{2+} in EF3. This Na^+-bound structure is of interest because EF2 assumes an octahedral geometry with four of the five loop residues and has an equatorial water molecule at the –Z position, bridging the ion with the 12^{th} residue (E85) of the EF hand loop. Interestingly, the other amino acids observed to change conformation in the $2Ca^{2+}$-structure do not change conformation with Na^+ bound to EF2.

EXPERIMENTAL PROCEDURES

Proteins

All proteins were expressed in and purified from T7 Express *Escherichia coli* (New England Biolabs) as described previously [14]. WT and mutant Rv proteins were prepared in the non-myristoylated form. The E153A Rv mutant was made using strand overlap extension PCR (Stratagene). RGS, the truncated RK mutant in which the catalytic domain is replaced with a GSGS linker joining residues 1-181 to 512-557 has been described [14]. RGS contains a C-terminal His_6 tag used for purification of the protein and for immobilization on a Ni-NTA matrix in the Rv/RK binding assays [14].

Ca^{2+}-binding assays

Ca^{2+}-binding assays were performed in triplicate according to previously established methods [11, 14] using a Hitachi F-2500 fluorescence spectrometer (Tokyo, Japan) to monitor Ca^{2+}-induced changes in intrinsic tryptophan fluorescence. Titration data were fit to a model for two independent sites

$$f\left(Ca^{2+}\right) = 0.5\left(\frac{\left[Ca^{2+}\right]}{\left[Ca^{2+}\right]+K_1}+\frac{\left[Ca^{2+}\right]}{\left[Ca^{2+}\right]+K_2}\right) \quad (1)$$

where $[Ca^{2+}]$ is the free Ca^{2+} concentration, $f(Ca^{2+})$ is the fraction of total sites occupied by Ca^{2+}, and K_1 and K_2 are the first and second dissociation constants, respectively.

RK-binding assays

The ability of Rv to bind RK was determined using RGS in a “pull-down assay” on a Ni-NTA column [14]. A more quantitative ITC assay was employed to determine the K_D for the Rv-RGS interaction using a nanoITC microcalorimeter (TA Instruments). WT or E153A Rv was first dialyzed 1:1000 against two changes of buffer (10 mM Tris (pH 7), 100 mM KCl, 10 mM $CaCl_2$) at 4 °C. Rv was loaded into the sample syringe (320-325 μM) and titrated into the RGS sample (29 μM) as 2 μL aliquots at 10 °C. Titration data were corrected for the heats of injection and dilution.

Rv crystallization, X-ray data collection, and data analysis

E153A Rv was crystallized in the presence of 20 mM $CaCl_2$ as described before [14], except that crystallization conditions, defined by the number and type of ions bound, were: $2Ca^{2+}$, 2.5 M ammonium sulfate (pH 6.5); and $1Na^{+}/1Ca^{2+}$, 1.3 M sodium citrate (pH 6.6). Crystals were soaked in reservoir solution containing 10% glycerol as a cryoprotectant before flash freezing with liquid nitrogen. Diffraction data were collected at the Advance Light Source (Lawrence Berkeley National Laboratory, Berkeley, CA). Data processing and refinement were performed as described previously [14]. WT Rv structure (PDB ID: 4MLW) was used as a search model for both structures described in this paper. Both data sets were refined anisotropically in the final refinement step using phenix.refine [16] from the PHENIX software suite v1.9 [17]. In the $2Ca^{2+}$ data set, hydrogens were generated in riding positions for protein atoms alone during final refinement. The data collection and final refinement statistics are given in Table 1. The coordinates and structure factors for the $2Ca^{2+}$ (PDB ID code 4YI8) and $1Na^{+}/1Ca^{2+}$ (PDB ID code 4YI9) data sets have been submitted to the Protein Data Bank. All the crystal structure figures in this paper were prepared using PyMol v1.3 (Schrödinger LLC, Portland, OR).

RESULTS

Characterization of the E153A Rv mutant

Given that Rv is a monomer in solution, and E153 is located on the surface of the protein well away from any of the active sites (Fig. 1), we did not expect RK- or Ca^{2+}-binding functions to be significantly impacted in the E153A crystal contact mutant. Nonetheless, it

was important to make this determination experimentally. Ca^{2+}-binding measurements were performed by monitoring the changes in intrinsic tryptophan fluorescence as a function of increasing Ca^{2+} concentration [11, 14, 18]. Titration data for WT Rv were fit well by equation 1, which models the binding of Ca^{2+} as two independent, non-cooperative events. Dissociation constants of 0.08 ± 0.01 μM and 7.8 ± 1.2 μM were determined for the high (EF3) and low (EF2) affinity sites, respectively (Fig. 2A) and are consistent with values reported in the literature [11, 15]. Dissociation constants determined for the high and low affinity sites of E153A Rv were 0.12 ± 0.01 μM and 13 ± 1.7 μM, respectively (Fig. 2B), demonstrating that the E153A mutation does not significantly affect Ca^{2+}-binding properties of the protein.

We next tested the ability of E153A Rv to bind RK, as monitored through the interaction with the RK RGS domain, which contains the N-terminal helix of RK that is targeted by Rv [6, 7]. This interaction was monitored both qualitatively with a pull-down assay (Fig. 2C) and quantitatively by ITC (Fig. 2, D and E). Both assays (Fig. 2, C and E) show that E153A Rv and RGS form a stable complex with 1:1 stoichiometry and a K_D of 1.0 μM, similar to that of WT Rv and RGS (1:1 stoichiometry, K_D = 1.3 μM; Fig. 2, C and D), demonstrating that the mutation has minimal effect on the binding of RK.

Crystal structure of E153A Rv with two bound Ca^{2+} ions

The E153A mutant crystallized in 2.5 M ammonium sulfate, and the crystal diffracted to 1.2 Å resolution. The refined electron density map clearly revealed that the EF2 loop was in the predicted closed conformation and coordinated an ion with heptacoordinate pentagonal bipyramidal geometry. The EF2 ion presented as a clear spherical F_o - F_c peak (35 σ) and was coordinated by an axial water molecule (−X) and five residues: D74 (X), N76 (Y), D78 (Z), T80 (main chain carbonyl oxygen; −Y), and E85 (−Z). Moreover, the EF2 density is similar to the density observed for a Ca^{2+} ion in EF3 (Fig. 3). The anomalous difference Fourier map, recorded with X-rays of 1.9 Å wavelength (data not submitted), for the Ca^{2+} in both EF2 and EF3 was observed up to 20 σ. As guided by the electron density, the EF2 loop was built in a closed conformation using Coot v0.7 [19] and a Ca^{2+} ion was included in both EF hands for further refinement. The final average B-factor for EF2 (all atoms; 14.4 $Å^2$) and EF3 (all atoms; 13.3 $Å^2$) indicated that both EF hands were highly stable. The axial water molecule coordinating Ca^{2+} in EF3 was observed in alternate positions, exhibiting an occupancy of 80% for the position shown in the figure.

Comparison of the E153A crystal structure with that of WT Rv (PDB ID: 4MLW) shows clear conformational changes for several residues (Fig. 4A). The fact that Ca^{2+} is bound to EF3 in both structures implies that all differences likely result from the binding of Ca^{2+} to EF2. Closing of the EF2 loop results in a ~3.7 Å inward shift of F73 that disrupts a hydrogen bond between the Nε1 of W104 and the Oγ atom of S72 (Fig. 4B). The bulky side chain of W104 is flipped ~100° towards M92 to reduce the steric hindrance from the shifted F73. M92 then undergoes a conformational change that makes room for the H91 side chain and a water molecule that stabilizes H91 by bridging it and the carbonyl oxygen of I88. The new conformation of H91 allows F23 to move 3.8 Å inward and, as a result of the shift,

allows rearrangement of the N-terminal region (residues 7-25) with a 20° tilt and 4.2 Å outward shift of the N-terminal helix (residues 11-19).

Reorientation of W104 provides a structural explanation for at least part of the observed fluorescence increase in the solution Ca^{2+}-titrations described above for the low-affinity site (K_2 ~8 μM), which has been assigned as EF2 through mutagenesis studies [10, 12] (Fig. 2, A and B).

Crystal structure of E153A Rv with one Na^+ and one Ca^{2+} bound

Crystals of E153A Rv were also grown in 1.3 M sodium citrate and diffracted to a resolution of 1.35 Å. The initial refinement revealed that the EF2 loop was in a partially closed conformation, but with three clear spherical F_o - F_c peaks (9 σ and two 5 σ values) at the center of EF2. We modeled these densities as a Na^+ ion and two water molecules, respectively. Assignment of the 9 σ density as Na^+ is supported by the following: First, the ion is coordinated with only four of the five residues of a typical EF hand: D74 (X), N76 (Y), D78 (Z), and T80 (main chain carbonyl oxygen; −Y) (Fig. 5A). One water molecule occupies the typical axial position (−X), but the second water was equatorial in the –Z position and bridged the Na^+ ion with E85. The bidentate carboxylate of E85 is required to complete coordination of a Ca^{2+} ion with a pentagonal bipyramidal geometry in the –Z position (Fig. 5A). This equatorial water provides only a single coordination that results in an octahedral geometry for the ion. Distances between the ion and loop residues are typical of metal ions bound within an EF hand (2.2-2.5 Å). Second, the F_o - F_c peak of the EF2 ion (9 σ) is significantly weaker than that of the Ca^{2+} ion coordinated in EF3 (18 σ). The anomalous difference Fourier map, recorded with X-rays of 1.9 Å wavelength (data not submitted), for the EF2 ion is also very weak compared to that of EF3 and even weaker than the sulphur atoms of residues C39, M92 and M132. Third, the final average B-factor for EF2 (all atoms; 25.0 $Å^2$) is higher than the Ca^{2+}-bound EF3 (all atoms; 20.8 $Å^2$), which indicates that EF2 assumes a less stable conformation than EF3. Fourth, refinement of the 9 σ density with either a Ca^{2+} ion or water molecule resulted in a higher or lower B-factor, respectively, than the coordinating residues. Fifth, with the exception of a ~2.7 Å inward shift of F73, none of the other residues observed to undergo conformational changes in the $2Ca^{2+}$ structure were observed to undergo changes in this structure. That is to say the W104-S72 hydrogen bond is intact (see above) and the bound EF2 ion is incapable of disrupting this bond because of the hexacoordinate geometry. Finally, the crystal was grown in 1.3 M sodium citrate. Titration of Rv with Ca^{2+} in the presence of 1.5 M sodium chloride shows the protein to have significantly decreased affinity for Ca^{2+} (K_1 = 19 ± 2.7 μM and K_2 = 500 ± 66 μM; Figure S1). The effect could even be exacerbated by citrate in the crystallization solution as a result of chelating free Ca^{2+}.

DISCUSSION

In over twenty years of study, Rv has heretofore never been crystallized with Ca^{2+} ions bound to both functional EF hands in the protein, and, in particular, Ca^{2+} was never observed coordinated to EF2 in the N-terminal domain of the protein. In an attempt to understand this, we screened published structures of the protein for the presence of crystal

contacts that might preclude coordination of a Ca^{2+} ion to EF2. With only one exception (*vide infra*), we found that each published structure contained an intermolecular crystal contact involving T80 of the EF2 loop. In each case, the contact involved hydrogen bonds from the main chain N-H and side chain –OH of a T80 donor from one Rv molecule and a carboxylate oxygen of an E153 acceptor from a second Rv molecule in the unit cell. E153 is distant from any of the known active site regions of the protein and, for this reason, was chosen as the site of mutation to see if coordination of Ca^{2+} in the EF2 loop of the altered protein was now permitted in the crystal. As anticipated, the E153A Rv mutant displayed near WT affinity for both Ca^{2+} ions and RK when assayed in solution (Fig. 2). In contrast, the crystal properties of the mutant protein were significantly different from the WT. Crystals of E153A were generally more numerous, larger (roughly 0.1 × 0.36 × 0.4 mm *versus* 0.08 × 0.1 × 0.2 mm), and diffracted to higher resolution (1.2 Å *versus* 1.45 Å) than those of WT Rv. Most significantly, the E153A mutant crystalized with two Ca^{2+} ions bound to the protein, one each in EF hands 2 and 3, and both EF hands conform to the canonical heptacoordinate pentagonal bipyramidal geometry expected for an EF hand when Ca^{2+} is bound (Fig. 3).

With one exception, all previous crystal structures of Rv contain the E153-T80 crystal contact that disrupts the binding of Ca^{2+} in EF2 (Table 2). The only exception, that of the C-terminally truncated (Δ191-202) mutant of Rv, exhibits no interaction between T80 and E153 in the crystal, possibly due to a different space group ($P2_1$) than other Rv proteins (I_4), and therefore, we would expect this crystal to bind Ca^{2+} at both sites in the protein. However, while the EF2 loop is partially closed in the Δ191-202 mutant, it is empty [15]. Notably, the Δ191-202 mutant was crystallized from 2.4 M sodium malate, and we suspect that malate chelates Ca^{2+} under these conditions much as we suggest citrate does with our E153A mutant crystallized from 1.3 M sodium citrate.

Inspection of the NMR structure (PDB ID: 2I94) of Rv with a bound peptide composed of the N-terminal residues of RK provides insight into the biological relevance of changes observed in the $2Ca^{2+}$ E153A crystal structure (Fig. 6). Several residues within our $2Ca^{2+}$ E153A Rv structure adopt a different conformation than has been seen in any other crystal structure of Rv (Fig. 4), forming a cascade of side-chain rearrangements beginning with the disruption of a hydrogen bond between S72 and W104 caused by an inward movement (3.7 Å) of F73 upon the binding of Ca^{2+} to EF2 and ending 28 Å away along the surface of the protein, with movement of F23 away from a Trp residue, W31, that is in the active site responsible for binding RK. W31 itself does not move in the new structure, most likely because it is involved in a tight interaction with I173 of a neighboring Rv molecule in the same unit cell. The interaction between W31 of Rv and F15 of RK is of particular interest because these residues are in *van der Waals* contact in all of the NMR structures. In addition, mutation of F15 (to A) in the RK peptide is known to disrupt the interaction with Rv[6, 7], indicating that F15 is critical for this interaction. Clearly the side-chain rearrangements observed with the E153A mutant highlight an allosteric path connecting the Ca^{2+}-binding site of EF2 to the RK-binding pocket. In this context, we note that the side-chain rearrangements observed in the $2Ca^{2+}$ E153A Rv structure do not occur in the $1Na^{+}/1Ca^{2+}$ E153A structure, increasing confidence that the conformational transition is

involved in enabling the binding of RK. In addition, it emphasizes the requirement for Ca^{2+} in EF2 to provide a trigger for the inward movement of F73 and subsequent side-chain rearrangements of amino acids involved in the allosteric conformational change. In this regard, the $1Na^{+}/1Ca^{2+}$ crystal structure is reminiscent of the calmodulin CaM41/75 mutant that in disulfide trapped form binds Ca^{2+} with hexacoordinate octahedral geometry in site 1 and cannot undergo the change to an active conformation [20, 21].

Supplementary Material

Refer to Web version on PubMed Central for supplementary material.

ACKNOWLEDGEMENTS

We thank Chris Miller for the use of his NanoITC and Ming-Feng Tsai for help with the ITC experiments. We are grateful to the staff at the Advanced Light Source-Berkeley Center for Structural Biology for their assistance in X-ray data collection. The Advanced Light Source is funded by the Director, Office of Science, Office of Basic Energy Sciences, of the United States Department of Energy under contract DE-AC02-05CH11231. The Berkeley Center for Structural Biology is supported in part by grants from the NIGMS, National Institutes of Health.

FUNDING SOURCE

This work was supported by the National Institutes of Health grants EY009514 and EY007965 to DDO.

ABBREVIATIONS

Rv	recoverin
Ca^{2+}	calcium
NCS	Neuronal calcium sensor
RK	rhodopsin kinase
WT	wild-type
RGS	regulator of G protein signaling
Ni-NTA	nickel-nitrilotriacetic acid
ITC	isothermal titration calorimetry
PDB	Protein Data Bank

REFERENCES

[1]. Burgoyne RD, Haynes LP. Understanding the physiological roles of the neuronal calcium sensor proteins. Molecular Brain. 2012; 5

[2]. Ames JB, Lim S. Molecular structure and target recognition of neuronal calcium sensor proteins. Biochim. Biophys. Acta. 2012; 1820:1205–1213. [PubMed: 22020049]

[3]. Klenchin VA, Calvert PD, Bownds MD. Inhibition of Rhodopsin Kinase by Recoverin: Further Evidence for a Negative Feedback System in Phototransduction. J. Biol. Chem. 1995; 270:16147–16152. [PubMed: 7608179]

[4]. Chen C-K, Inglese J, Lefkowitz RJ, B. HJ. Ca2+ Dependent Interaction of Recoverin with Rhodopsin Kinase. J. Biol. Chem. 1995; 270:18060–18066. [PubMed: 7629115]

[5]. Kawamura S. Rhodopsin phosphorylation as a mechanism of cyclic GMP phosphodiesterase regulation by S-modulin. Nature. 1993; 362:855–857. [PubMed: 8386803]

[6]. Ames JB, Levay K, Wingard JN, Lusin JD, Slepak VZ. Structural Basis for Calcium-induced Inhibition of Rhodopsin Kinase by Recoverin. J. Biol. Chem. 2006; 281:37237–37245. [PubMed: 17020884]

[7]. Higgins MK, Oprian DD, Schertler GF. Recoverin Binds Exclusively to an Amphipathic Peptide at the N-Terminus of Rhodopsin Kinase, Inhibiting Rhodopsin Phosphorylation without Affecting Catalytic Activity of the Kinase. J. Biol. Chem. 2006; 281:19426–19432. [PubMed: 16675451]

[8]. Palczewski K, Buczylko J, Lebioda L, Crabb JW, Polans AS. Identification of the N-terminal Region in Rhodopsin Kinase Involved in Its Interaction with Rhodopsin. J. Biol. Chem. 1993; 268:6004–6013. [PubMed: 8383684]

[9]. Flaherty KM, Zozulya S, Stryer L, McKay DB. Three-dimensional structure of recoverin, a calcium sensor in vision. Cell. 1993; 75:709–716. [PubMed: 8242744]

[10]. Senin II, Fischer T, Komolov KE, Zinchenko DV, Phillipov PP, Koch WJ. Ca2+-Myristoyl Switch in the Neuronal Calcium Sensor Recoverin Requires Different Functions of Ca2+-binding Sites. J. Biol. Chem. 2002; 277:50365–50372. [PubMed: 12393897]

[11]. Ames JB, Prorumb T, Tanaka T, Ikura M, Stryer L. Amino-terminal Myristoylation Induces Cooperative Calcium Binding to Recoverin. J. Biol. Chem. 1995; 270:4526–4533. [PubMed: 7876221]

[12]. Alekseev AM, Shulga-Morskoy SV, Zinchenko DV, Shulga-Morskaya SA, Suchkov DV, Vaganova SA, Senin II, Zargarov AA, Lipkin VM, Akhtar M, Philippov PP. Obtaining and characterization of EF-hand mutants of recoverin. FEBS Lett. 1998; 440:116–118. [PubMed: 9862438]

[13]. Weiergräber OH, Senin II, Phillipov PP, Granzin J, Koch K-W. Impact of N-terminal Myristoylation on the Ca2+-dependent Conformational Transition in Recoverin. J. Biol. Chem. 2003; 278:22972–22979. [PubMed: 12686556]

[14]. Ranaghan MJ, Kumar RP, Chakrabarti KS, Buosi V, Kern D, Oprian DD. A Highly Conserved Cysteine of Neuronal Calcium-sensing Proteins Controls Cooperative Binding of Ca2+ to Recoverin. J. Biol. Chem. 2013; 288:36160–36167. [PubMed: 24189072]

[15]. Weiergräber OH, Senin II, Zernii EY, Churumova VA, Kovaleva NA, Nazipova AA, Permyakov SE, Permyakov EA, Philippov PP, Granzin J, Koch K-W. Tuning of a Neuronal Calcium Sensor. J. Biol. Chem. 2006; 281:37594–37602. [PubMed: 17015448]

[16]. Afonine PV, Grosse-Kunstleve RW, Echols N, Headd JJ, Moriarty NW, Mustyakimov M, Terwilliger TC, Urzhumtsev A, Zwart PH, Adams PD. Towards automated crystallographic structure refinement with phenix.refine. Acta Cryst. 2012; D68:352–367.

[17]. Adams PD, Afonine PV, Bunkoczi G, Chen VB, Davis IW, Echols N, Headd JJ, Hung LW, Kapral GJ, Grosse-Kunstleve RW, Kunstleve RW, McCoy AJ, MOriarty NW, Oeffner R, Read RJ, Richardson DJ, Richardon JS, Terwilliger TC, Zwart PH. PHENIX: A comprehensive Python-based system for macromolecular structure solution. Acta Cryst. 2010; D66:213–221.

[18]. Baldwin AN, Ames JB. Core Mutations That Promote the Calcium-INduced Allosteric Transidtion of Bovine Recoverin. Biochemistry. 1998; 37:17408–17419. [PubMed: 9860856]

[19]. Emsley P, Lohkamp B, Scott W, Cowtan K. Features and Development of Coot. Acta Cryst. 2010; D66:486–501.

[20]. Tan RY, Mabuchi Y, Grabarek Z. Blocking the Ca2+-induced conformational transitions in calmodulin with disulfide bonds. J Biol Chem. 1996; 271:7479–7483. [PubMed: 8631777]

[21]. Grabarek Z. Structure of a trapped intermediate of calmodulin: calcium regulation of EF-hand proteins from a new perspective. J Mol Biol. 2005; 346:1351–1366. [PubMed: 15713486]

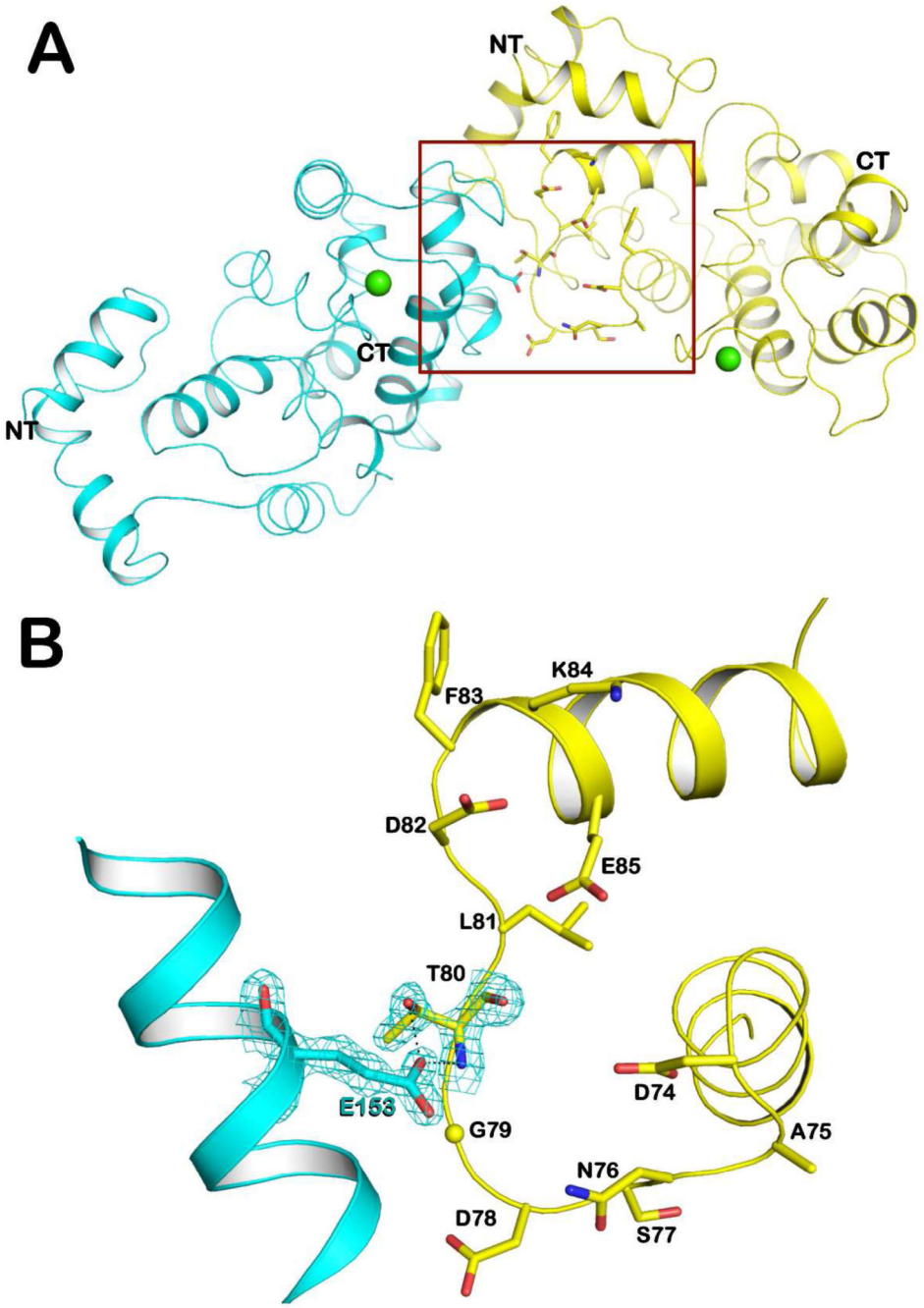

FIGURE 1.

(A) Intermolecular crystal contact between Rv molecules. The N-terminus (NT), C-terminus (CT), and Ca^{2+} ion coordinated in EF3 (green sphere) are shown for each molecule of Rv (PDB ID: 4MLW). (B) Close up of the intermolecular hydrogen bond between E153 and T80 of WT Rv. The $2F_0$-F_C electron density map is shown at a 2 σ cut off for residues E153 and T80.

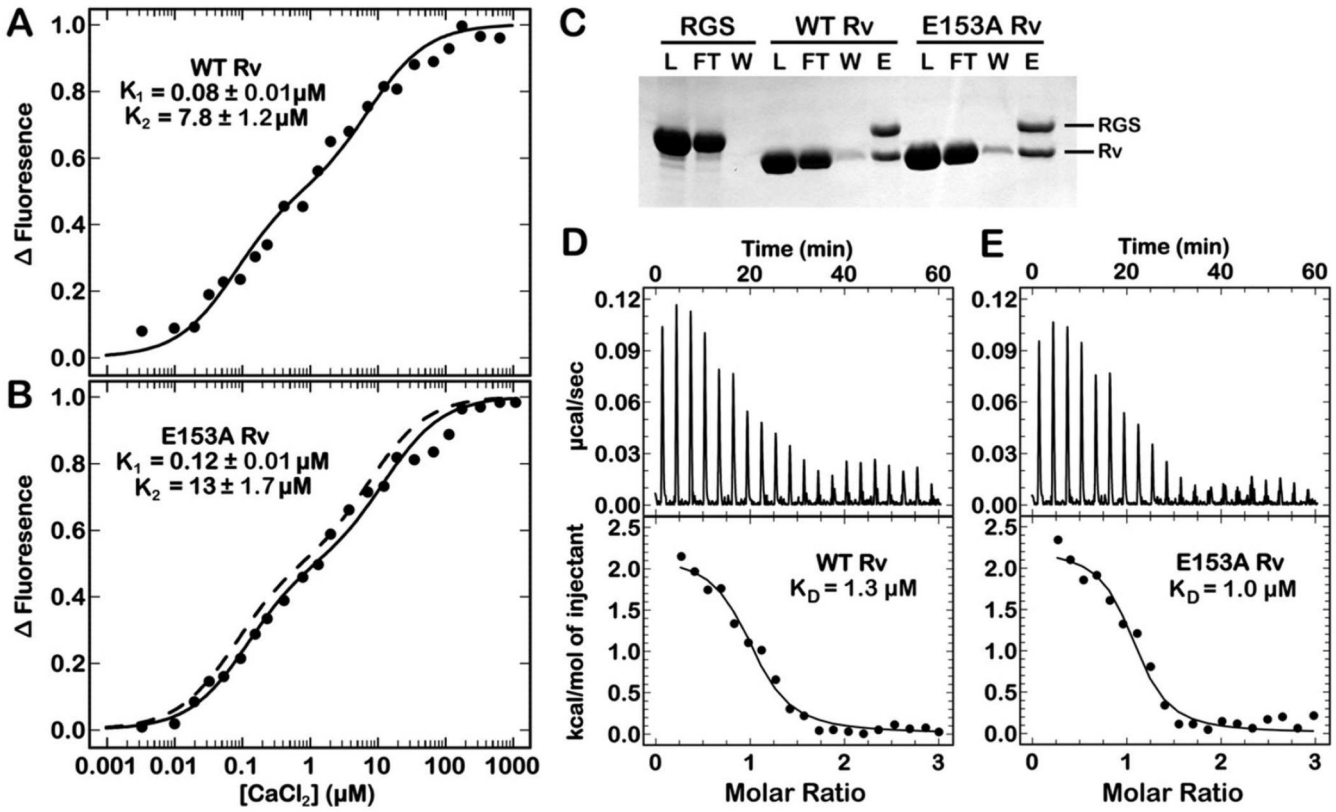

FIGURE 2.

Ca^{2+} and RGS binding assays for WT and E153A Rv. (A) Normalized change in fluorescence for Ca^{2+} binding to WT Rv. Equation 1 was used to fit the titration data. (B) Normalized change in fluorescence for Ca^{2+} binding to E153A Rv. Equation 1 was used to fit the titration data, and the *dashed line* is the titration curve for WT Rv from Fig. 2A. (C) Pull-down assay in which RGS was first immobilized on Ni-NTA matrix before Rv was added in the presence of 1 mM $CaCl_2$. After binding, each sample was washed with 25 column volumes of buffer and the Rv-RGS complex was eluted with 250 mM imidazole. Lanes are defined as L, load; FT, flow-through; W, last wash; and E, elution. (D) ITC isotherm showing the heat measured when WT Rv (325 μM) was titrated into a solution of RGS (29 μM) at 10°C. (E) ITC isotherm showing the heat measured when E153A Rv (320 μM) was titrated into a solution of RGS (29 μM) at 10°C.

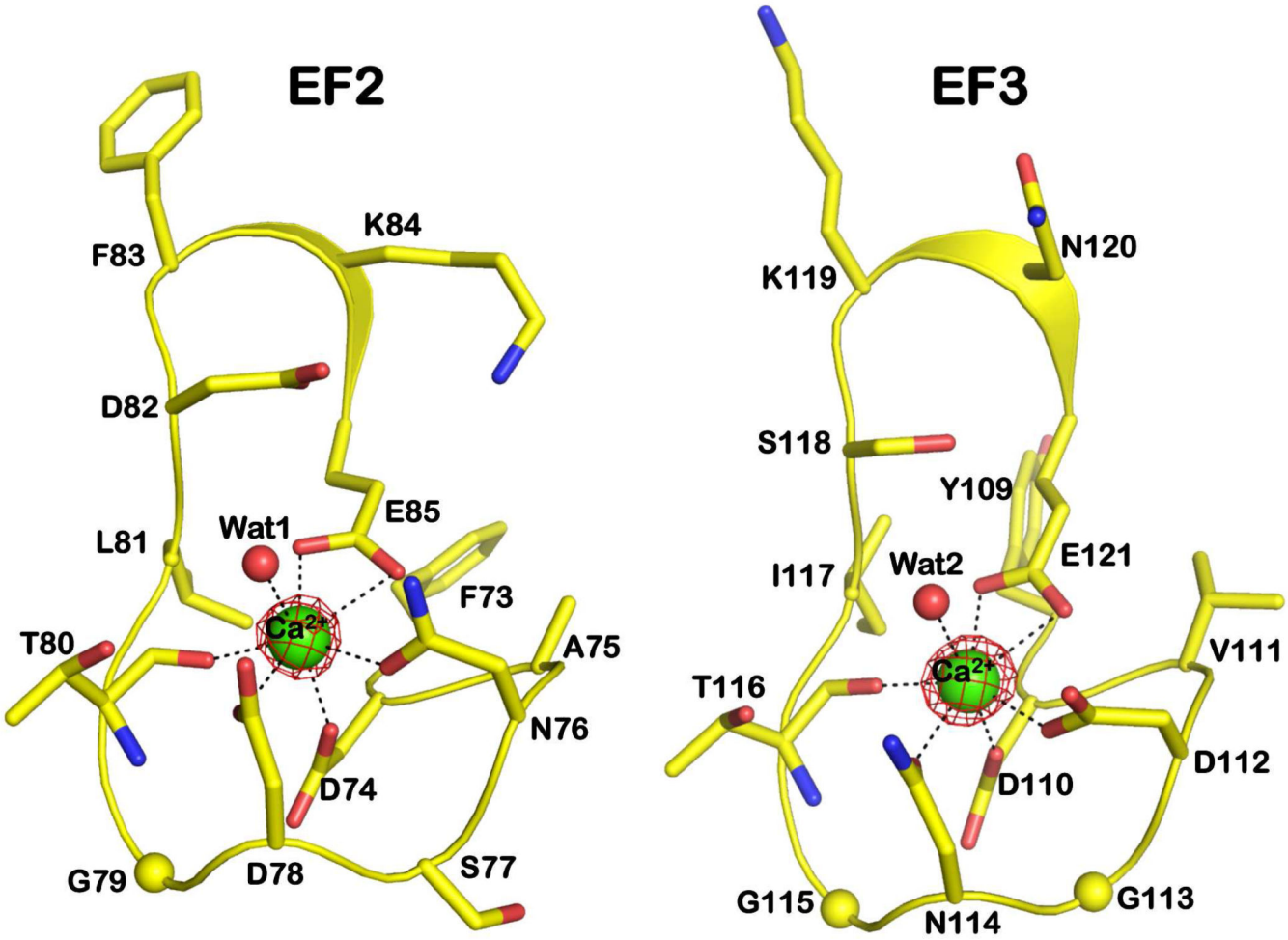

FIGURE 3.

Structures showing the coordination of a Ca^{2+} ion in EF2 and EF3. The F_0 - F_C omit map is shown for both Ca^{2+} ions at a 5 σ cut off.

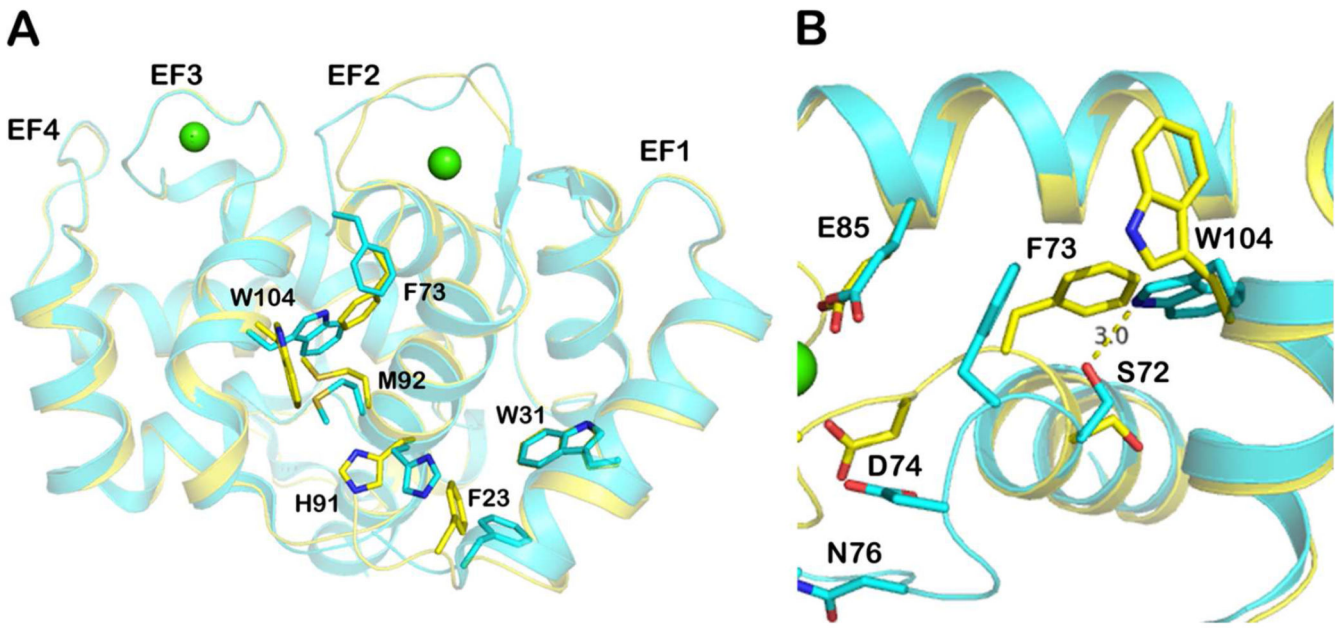

FIGURE 4.

Superimposed structures of WT (*cyan*; PDB ID: 4MLW) and E153A (*yellow*; PDB ID: 4YI8) Rv. (A) Residues altered by the binding of Ca^{2+} (*green spheres*) in EF2 are shown as sticks. The N-terminal tail (residues 7-20) has been removed to aid visualization of the highlighted residues. (B) Close up image showing how Ca^{2+}-binding in EF2 shifts F73 to disrupt the S72-W104 hydrogen bond that initiates the rearrangement shown in Fig. 4A.

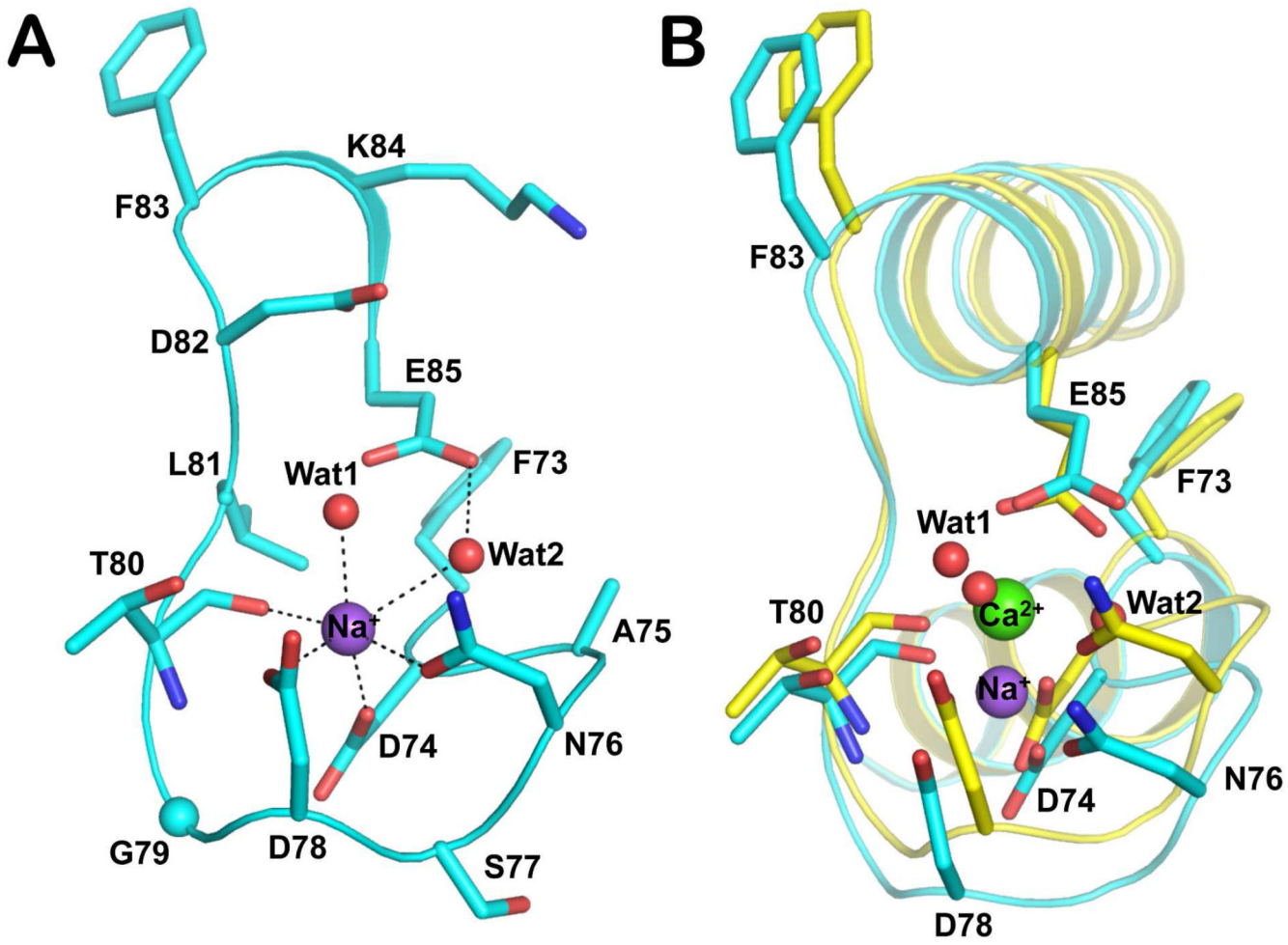

FIGURE 5.

(A) Structure showing the coordination of a Na^+ ion in EF2 of E153A Rv. (B) Superposition of EF2 of E153A Rv that coordinates either a Ca^{2+} ion (yellow colored backbone with light green sphere) or a Na^+ ion (green colored backbone with purple sphere).

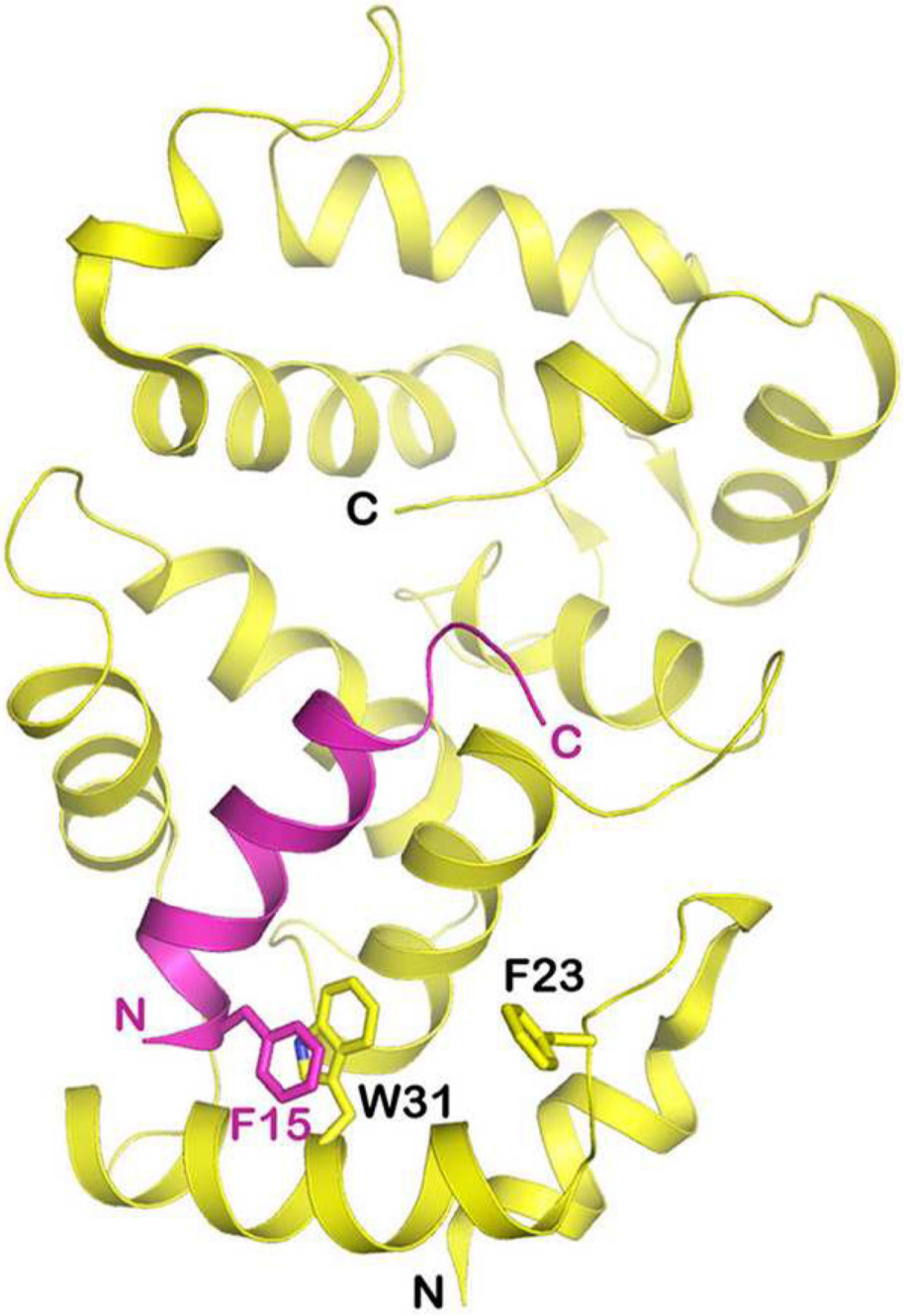

FIGURE 6.

NMR Models (PDB ID: 2I94) of the N-terminal 15 residues of RK (magenta) binding to Rv (yellow). Schematic showing the arrangement of F23 and W31 of Rv with F15 of RK.

Table 1

Data collection and refinement statistics

	$2Ca^{2+}$	**$1Na^{+}/1Ca^{2+}$**
PDB ID	4YI8	4YI9
Data collection statistics		
Space group	I4	I4
Resolution range (Å)	48 - 1.20	32 - 1.35
Highest resolution shell (Å)	1.26 - 1.20	1.42 - 1.35
Unit cell parameters (Å)	a = b = 84.2, c = 59.2	a = b = 85.3, c = 58.8
Total reflections	471180	257297
Unique reflections	64447	45091
Completeness %[a]	99.9 (99.1)	97.3 (85.6)
R_{merge} %[a]	6.8 (34.6)	4.3 (47.7)
I/σ (I)[a]	17.3 (3.9)	18.0 (2.8)
Redundancy	7.3 (4.7)	5.7 (4.5)
Refinement statistics		
Resolution range (Å)	48 - 1.20	32 - 1.35
No. of reflections used	64442	45052
R_{cryst} %	12.1	15.2
R_{free} %	14.0	17.4
Protein atoms	1650	1627
Metal atoms	2 Ca^{2+}	1 Ca^{2+}, 1 Na^{+}
Water molecules	234	223
r.m.s.d. in bond lengths (Å)	0.01	0.01
r.m.s.d. in bond angles (°)	1.3	1.0

[a]Highest resolution cell values are given parenthesis.

Table 2

Summary of available Rv crystal structures listed in the Protein Data Bank

PDB	Resolution (Å)	Mutant	# Ca^{2+} ions	Organism	Crystallization condition	Reference
1REC	1.9	WT	1	Bos taurus	70%-90% saturated ammonium sulfate, 1 mM $CaCl_2$	9
1OMR	1.5	WT	1	Bos taurus	70%-90% saturated ammonium sulfate, 100 mM TRIS, pH 8, 1 mM $CaCl_2$, 1 mM $MgCl_2$	13
1OMV	1.9	E85Q	1	Bos taurus		
2HET	3.0	Δ191-202	1	Bos taurus	2.4 M sodium malonate, 2 mM $CaCl_2$, pH 7.0	15
2D8N	2.2	WT	0	Homo sapiens	1.2 M sodium citrate, 100 mM sodium HEPES, pH7.5	Unpublished
4MLW	1.45	WT	1	Bos taurus	1.8 M ammonium citrate, pH 7.0, 1-5 mM $CaCl_2$	14
4M2Q	1.9	WT (Sulfenic acid-39)	1	Bos taurus		
4M2O	1.5	C39A	1	Bos taurus	2.0 M ammonium citrate, pH 7.0, 1-5 mM $CaCl_2$	
4M2P	1.45	C39D	1	Bos taurus	2.4 M sodium malonate, pH 7.0, 1-5 mM $CaCl_2$	
4YI9	1.35	E153A	1	Bos taurus	1.3 M sodium citrate, pH 6.6, 20 mM $CaCl_2$	This work
4YI8	1.2	E153A	2	Bos taurus	2.5 M ammonium sulfate, pH 6.5, 20 mM $CaCl_2$	